JOURNAL OF GEOPHYSICAL RESEARCH, VOL. 113, D03202, doi:10.1029/2007JD009054, 2008

Global and temporal distribution of meteoric smoke: A two-dimensional simulation study

L. Megner,[1] D. E. Siskind,[2] M. Rapp,[3] and J. Gumbel[1]

Received 8 June 2007; revised 12 October 2007; accepted 26 October 2007; published 2 February 2008.

[1] Meteoric material entering Earth's atmosphere ablates in the mesosphere and is then expected to recondense into tiny so-called ''smoke particles.'' These particles are thought to be of great importance for middle atmosphere phenomena like noctilucent clouds, polar mesospheric summer echoes, metal layers, and heterogeneous chemistry. Commonly used one-dimensional (1-D) meteoric smoke profiles refer to average global conditions and yield of the order of a thousand nanometer sized particles per cubic centimeter at the mesopause, independent of latitude and time of year. Using the first two-dimensional model of both coagulation and transport of meteoric material we here show that such profiles are too simplistic, and that the distribution of smoke particles indeed is dependent on both latitude and season. The reason is that the atmospheric circulation, which cannot be properly handled by 1-D models, efficiently transports the particles to the winter hemisphere and down into the polar vortex. Using the assumptions commonly used in 1-D studies results in number densities of nanometer sized particles of around 4000 cm^{-3} at the winter pole, while very few particles remain at the Arctic summer mesopause. If smoke particles are the only nucleation kernel for ice in the mesosphere this would imply that there could only be of the order of 100 or less ice particles cm^{-3} at the Arctic summer mesopause. This is much less than the ice number densities expected for the formation of ice phenomena (noctilucent clouds and polar mesospheric summer echoes) that commonly occur in this region. However, we find that especially the uncertainty of the amount of material that is deposited in Earth's atmosphere imposes a large error bar on this number, which may allow for number densities up to 1000 cm^{-3} near the polar summer mesopause. This efficient transport of meteoric material to the winter hemisphere and down into the polar vortex results in higher concentrations of meteoric material in the Arctic winter stratosphere than previously thought. This is of potential importance for the formation of the so-called stratospheric condensation nuclei layer and for stratospheric nucleation processes.

Citation: Megner, L., D. E. Siskind, M. Rapp, and J. Gumbel (2008), Global and temporal distribution of meteoric smoke: A two-dimensional simulation study, *J. Geophys. Res.*, *113*, D03202, doi:10.1029/2007JD009054.

1. Introduction

[2] Meteoroids reaching Earth's atmosphere are subject to strong deceleration and ablate mainly in the 75–120 km region whereupon the resulting material is believed to recondense to nanometer sized ''smoke particles'' [*Hunten et al.*, 1980; *Kalashnikova et al.*, 2000; *Plane*, 2004; *Janches and ReVelle*, 2005]. These particles are especially important in the middle atmosphere where dust sources from below are small. Smoke particles are thought to play a major role in a host of middle atmospheric phenomena, such as noctilucent clouds (NLCs), polar mesospheric summer echoes (PMSEs), metal layers, and heterogeneous chemistry controlling key species such as water vapor [*Turco et al.*, 1982; *Summers and Siskind*, 1999; *Plane*, 2000].

[3] Despite the obvious scientific interest in smoke particles, little is known about their actual properties, and a number of factors associated with meteoric smoke formation are poorly understood. This lack of knowledge is mainly due to the complications involved with measurements at mesospheric altitudes where in situ studies only can be carried out using sounding rockets [*Gelinas et al.*, 1998; *Croskey et al.*, 2001; *Rapp et al.*, 2005; *Schulte and Arnold*, 1992; *Lynch et al.*, 2005]. The detection of nanometer sized particles is especially problematic since the shock wave in front of the rocket may prevent small particles from reaching the detector [*Horanyi et al.*, 1999; *Rapp et al.*, 2005; *Hedin et al.*, 2007]. Although calculations of the aerodynamical effects on detection efficiencies were preformed 40 years ago when attempts first were made to collect micrometeoroids [*Kornblum*, 1970], these prob-

[1] Department of Meteorology, Stockholm University, Stockholm, Sweden.
[2] Space Science Division, Naval Research Laboratory, Washington, D. C., USA.
[3] Leibniz-Institute of Atmospheric Physics, Kühlungsborn, Germany.

0148-0227/08/2007JD009054$09.00

Report Documentation Page

Form Approved
OMB No. 0704-0188

1. REPORT DATE	2. REPORT TYPE	3. DATES COVERED
12 OCT 2007		**00-00-2007 to 00-00-2007**

4. TITLE AND SUBTITLE	5a. CONTRACT NUMBER
Global and temporal distribution of meteoric smoke: A two-dimensional simulation study	5b. GRANT NUMBER
	5c. PROGRAM ELEMENT NUMBER
6. AUTHOR(S)	5d. PROJECT NUMBER
	5e. TASK NUMBER
	5f. WORK UNIT NUMBER
7. PERFORMING ORGANIZATION NAME(S) AND ADDRESS(ES) **Naval Research Laboratory,Space Science Division,4555 Overlook Avenue SW,Washington,DC,20375**	8. PERFORMING ORGANIZATION REPORT NUMBER
9. SPONSORING/MONITORING AGENCY NAME(S) AND ADDRESS(ES)	10. SPONSOR/MONITOR'S ACRONYM(S)
	11. SPONSOR/MONITOR'S REPORT NUMBER(S)

12. DISTRIBUTION/AVAILABILITY STATEMENT
Approved for public release; distribution unlimited

13. SUPPLEMENTARY NOTES

14. ABSTRACT

15. SUBJECT TERMS

16. SECURITY CLASSIFICATION OF:			17. LIMITATION OF ABSTRACT	18. NUMBER OF PAGES	19a. NAME OF RESPONSIBLE PERSON
a. REPORT **unclassified**	b. ABSTRACT **unclassified**	c. THIS PAGE **unclassified**	**Same as Report (SAR)**	**15**	

lems have not been addressed in the majority of experiments aimed at measuring meteoric smoke.

[4] The size cutoff above which particles are detected is a complicated function of the shape of the rocket instrument, the density of the air, and the velocity of the rocket. Hence it is not trivial to estimate and varies greatly with altitude. Further, owing to difficulties in detecting neutral particles, measurements of nanometer sized particles in the mesosphere are so far only available for the charged fraction of the total particle population. Attempts to study smoke composition and to measure neutral as well as charged particles have recently been made by means of rocket-borne collection and subsequent laboratory analysis [*Gumbel*, 2005]. The analyses of the collected material is still in progress. In the stratosphere, direct measurements of meteoric smoke particles become troublesome because particles of terrestrial origin may reach these altitudes. There have been several balloon measurements of the so-called condensation nuclei layer (CN layer) made up of small submicron sized particles which potentially could be meteoric smoke [e.g., *Rosen and Hofmann*, 1983; *Hofmann*, 1985; *Testa et al.*, 1990]. However, it is difficult to determine if, or how much of, the particles are of terrestrial or extraterrestrial origin. Partly owing to the difficulties involved in measuring meteoric smoke particles, many of the factors that determine their global distribution are poorly known. These factors include the amount of meteoric input, the average charge of the particles and the nature of ablation and coagulation. As we shall see this feeds back to uncertainties in the particle population.

[5] Several model studies have been concerned with the extraterrestrial material and its interactions in the middle atmosphere. Before the idea of recondensed meteoric smoke had been brought forward, there were speculations regarding formation of noctilucent clouds directly on extraterrestrial dust. A simple two-dimensional (2-D) model was then used to determine the dust trajectories [*Fiocco and Grams*, 1971]. Owing to the lack of understanding of the wind field at this time, their model suggested that the transport toward the winter pole was restricted to altitudes below 80 km, thus not effecting the meteoric smoke distribution at NLC altitudes. After this, model studies have concerned the ablation process [*Hunten et al.*, 1980; *Kalashnikova et al.*, 2000] and the subsequent re-condensation and formation of smoke particles [*Hunten et al.*, 1980; *Gabrielli et al.*, 2004; *Megner et al.*, 2006]. However, all these studies have been undertaken using 1-D models. A recent sensitivity study [*Megner et al.*, 2006] shows that the background wind field of the atmosphere is the single most important factor in determining the smoke distribution. Obviously, a 1-D model treats background winds only in a simplistic way, and cannot describe the strong variations in wind field with latitude and season. Hence the resulting smoke distribution is not a good estimate of the real distribution at a particular location. In order to properly study the global smoke distribution, a multidimensional model is required, which appropriately can describe the mesospheric circulation, with updraft at the summer pole, transport toward the winter hemisphere and downwelling at the winter pole.

[6] Here we have developed a new 2-D model to study the transport and coagulation of meteoric material in the middle atmosphere as well as the resulting spatial and temporal variations in the smoke distribution. The model, which couples an atmospheric circulation model and a microphysical model, is described in section 2. This section also includes a study of the required number of size bins needed for an adequate description of the particle microphysics. A general case scenario of the global distribution of smoke particles at different times of the year is presented in section 3. Section 4 shows the general results if a seasonal variation of extraterrestrial input is included in the model. In section 5 we concentrate on two regions of particular interest, the Arctic summer mesopause and the Arctic winter stratosphere. We investigate the sensitivity of the smoke distributions in these regions to factors such as the amount of meteoric input, the coagulation efficiency, the size of the molecular clusters that are produced as a result of the ablation, the height of ablation and the residual wind field. Section 6 contains a study of how the meteoric material is transported and the timescales involved. In section 7 we discuss our results and their implications and compare them to experimental findings. Finally, the main conclusions are summarized in section 8.

2. Model Description

[7] The CARMA-CHEM2D (CC2D) model consists of a coupling between a two-dimensional chemical dynamical model, CHEM2D [*Siskind et al.*, 1997, 2003; *Summers et al.*, 1997], which is used to transport the material, and a microphysical model, CARMA (the Community Aerosol and Radiation Model for Atmospheres) [*Turco et al.*, 1979; *Toon et al.*, 1979], which is used to treat particle coagulation.

[8] The CHEM2D model is a complete chemical dynamical model which extends from the surface to approximately 115 km. The dynamical module uses the transformed Eulerian Mean formulation to represent the mean meridional circulation. Random motion of air particles owing to fluctuations in the wind field are parameterized using vertical mixing (K_{zz}). Sedimentation is calculated using the kinetic drag law [*Reid*, 1975]. The chemical module accounts for 45 species and 254 reactions. For this work we used a time step of 2 hours. *Siskind et al.* [2003] show how the model responds to changing gravity wave drag and solar insolation; their results were the first to posit a theoretical explanation for a possible N/S difference in Polar Mesospheric Cloud (PMC) occurrence frequency, which has now become well established [*Bailey et al.*, 2005]. *Siskind et al.* [2005] extended this model to make specific forecasts of PMC brightness variability as a function of latitude, hemisphere and solar activity. *Hervig and Siskind* [2006] validated aspects of this model against HALOE temperature data; other predictions of the model were not in agreement with the data. Thus, while the model got the sign of the N/S summer temperature difference correct, it overestimated the magnitude of the difference by about 5 K. The predicted solar cycle high-latitude temperature change of about 2 K was in good agreement with that seen by HALOE, but the predicted H2O change was too small (<5% below 80 km in contrast to an observed 10% change). Most recently, a crude interactive PMC parameterization has been added to CHEM2D [*Siskind and Stevens*, 2006; *Siskind et al.*, 2007]. This parameterization has demonstrated possible feedbacks of PMCs on their thermal and chemical environment. For

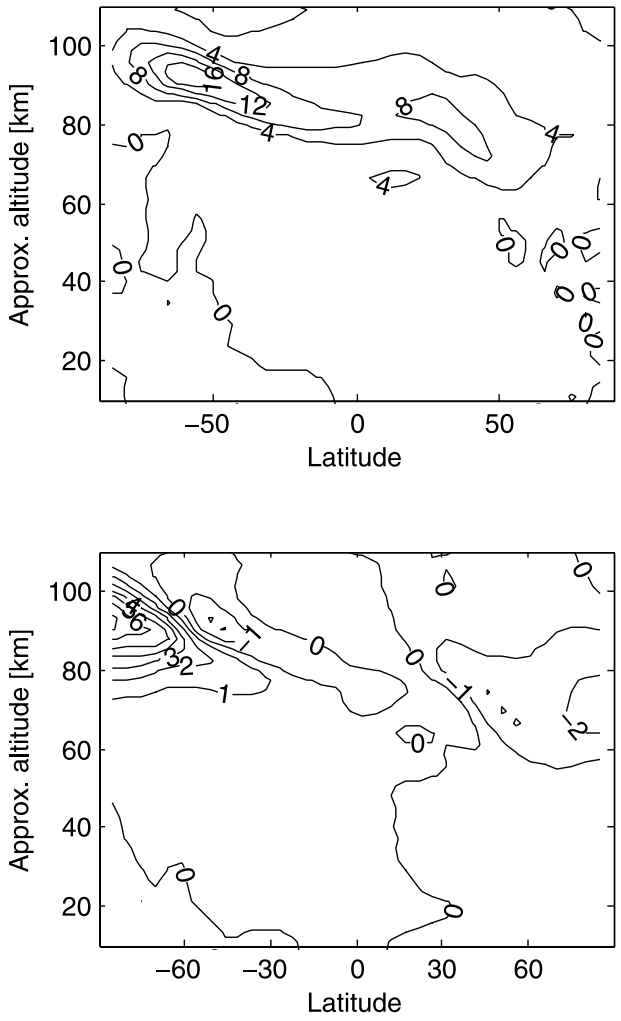

Figure 1. Residual wind field of the CHEM2D model for 27 December. (top) The meridional winds given in m/s, positive northward; (bottom) the vertical winds in cm/s, positive upward. The approximate altitude is calculated from the pressure level using a constant scale height of 7 km so that $z = -7\ \ln(p/1000)$ km, where p is the pressure in millibar. The characteristic middle atmospheric circulation, with a strong updraft at the summer pole, transport toward the winter hemisphere, and downwelling at the winter pole, is clearly seen.

example, *Siskind et al.* [2007] showed that HALOE ozone appears to be enhanced above PMCs and they suggest that this may be due to reduced HOx associated with dehydration. The residual wind field of the model is shown in Figure 1. The main features, i.e., the upwellings and downwellings at the poles and winds directed from summer to winter pole throughout the mesosphere with a maximum around 80–90 km depending on latitude, are in good agreement with several established models such as the Whole Atmosphere Community Climate Model (WACCM) [*Sassi et al.*, 2004], the Kühlungsborn Mechanistic general Circulation Model (KMCM) [*Becker and Fritts*, 2006] and the 3-D Canadian Middle Atmosphere Model (CMAM) [*McLandress et al.*, 2006].

[9] The CARMA model is a flexible, microphysical model which has been applied to a wide variety of atmospheric problems both on Earth and on other planets. The applications range from studies of tropospheric cirrus clouds [e.g., *Jensen et al.*, 2001], via polar stratospheric clouds [*Toon et al.*, 1989], up to studies of noctilucent clouds [e.g., *Rapp and Thomas*, 2006]. The model originated from a one-dimensional stratospheric aerosol code developed by *Turco et al.* [1979] and *Toon et al.* [1979], which included both gas phase sulfur chemistry and aerosol microphysics. In CC2D only the coagulation algorithm of CARMA is used. It was developed by *Toon et al.* [1988] and *Jacobson et al.* [1994] where it is described in detail. The scheme allows the computation of coagulation among any number of particle types but for the purpose of this study it is enough to treat meteoric smoke as one substance. The particles are treated as spherical and undergo coagulation as a result of collisions, mainly owing to Brownian motion. Coalescence is assumed and advection in radius space is computed using the piecewise parabolic method algorithm [*Colela and Woodard*, 1984]. The coagulation time step is 30 min. For a more thorough discussion of the modeling of meteoric smoke coagulation see *Megner et al.* [2006] and for more information on the numerical aspects of the CARMA model, see *Toon et al.* [1988].

[10] The CC2D model uses 28 radius size bins (or 14 radius bins in sections 6 and 5.1) ranging from 0.2 nm, which roughly corresponds to molecular sized particles, to 100 nm. The size bins increase geometrically. That is, the particle volume assigned to one bin is equal to that of the previous bin multiplied by a constant factor, V_{RAT} (V_{RAT} = 2.0 when 28 bins are used and V_{RAT} = 4.0 when 14 bins are used), so that the center radius of the ith bin is

$$r_i = r_1 V_{RAT}^{(i-1)/3} \tag{1}$$

where r_1 is the particle center radius of the first bin. The domain reaches from the ground to approximately 114 km with 2.66 km altitudinal and 4.9° latitudinal resolution. During the calculations the vertical coordinate is pressure, later converted to geometric altitudes using the hydrostatic equation. The technical coupling of the two submodels is done by first letting the CHEM2D model transport the particles for a simulation period of 2 hours, during which each size bin is transported separately, unable to react with other material. After this the CARMA model coagulates the particles, i.e., advects them between the size bins, for the same amount of simulation time.

[11] Ablated material, corresponding to a global amount of ablated meteoric material of 44 metric tonnes per day, is deposited evenly over the globe primarily at altitudes between 75 and 100 km, as described by an ablation profile calculated by *Kalashnikova et al.* [2000]. The amount of ablated material is proportional to the column density of the air that the meteoroid has traversed, i.e., the pressure level. The ablation profile is therefore taken to represent pressure altitudes rather than geometric altitudes. In agreement with *Hunten et al.* [1980] we assume a smoke material density of 2 g cm^{-3}. [*Rosinski and Snow*, 1961] argue that the concentration of the ablated material within the meteor trail is too low for direct re-condensation to compete with the

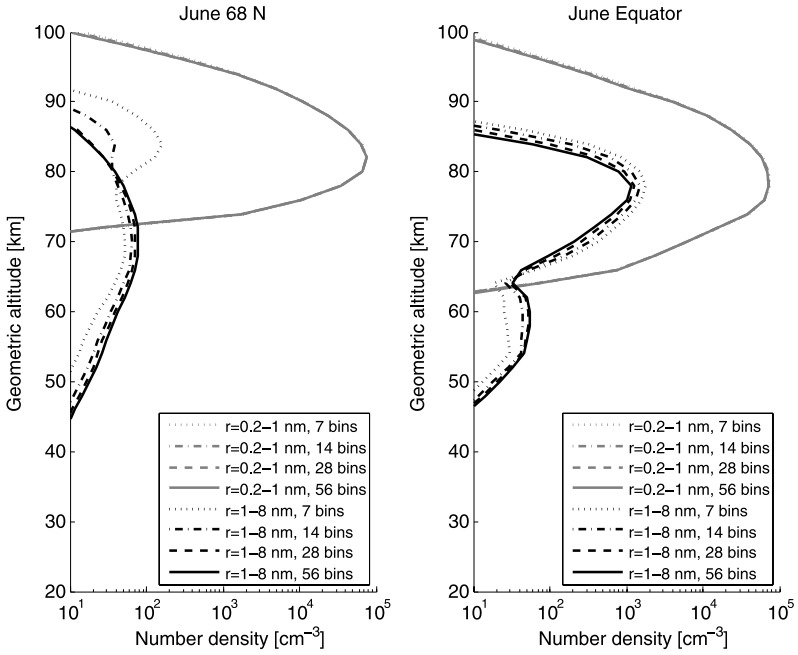

Figure 2. Number distribution of particles of different sizes as a result of model runs using different numbers of size bins. The 56-bin model is shown as a solid line, the 28-bin model as a dashed line, the 14-bin model as a dash-dotted line, and the 7-bin model as a dotted line. The gray lines show particles between 0.2 and 1 nm, and the black lines show particles between 1 and 8 nm.

outward diffusion of the meteor trail. A direct formation of meteoric smoke particles inside the trail is thus unlikely. Instead, condensation takes place on longer timescales (days) and, thus, atoms, molecules and molecular clusters formed in the ablation process become ''normal'' actors in the mesospheric gas phase chemistry. In the model freshly ablated material is therefore continuously fed into the smallest size bin, 0.2 nm radius, which roughly corresponds to molecular dimensions. Material only enters the model in this smallest size bin. As coagulation continues the material transfers to the bigger size bins, acquires a higher sedimentation speed, and eventually collects in the lowest-altitude bins. After the first year of running the model, a year-to-year ''steady state'' is reached for altitudes above 20 km, i.e., the amount of material entered in the smallest size bin equals the amount ultimately accumulated in the lowest-altitude bins, so that the meteoric smoke profile from year to year is roughly constant. Since meteoric smoke is not transported upward, this is equivalent to a boundary condition that removes the smoke particles once they have reached 20 km. The results shown in this paper are obtained by running the 28-bin CC2D model for 2 years, where the first year is considered a spin-up year and data is used only from the second year, when a ''steady state'' has been reached.

[12] Since all model studies involving coagulation of smoke particles so far have been conducted with 1-D models, computation time has not been a major concern. Hence the coagulation algorithms have been using much smaller radius size bins than we use in this study. When going to more dimensions, computation time becomes an issue, and larger steps between the size bins become a necessity. In order to understand the errors that a reduction of the amount of size bins infers, we ran our model using 7, 14, 28 and 56 size bins, all spanning the interval of 0.2 to 100 nm radius. Figure 2 shows the resulting smoke particle distribution for June conditions at 68°N and the equator. The gray lines show the particles smaller than 1 nm radius and the black lines show the particles with radii between 1 and 8 nm. The solid lines show the result using 56 size bins and the dashed, dashed-dotted and dotted lines show the result using 28, 14 and 7 size bins correspondingly. We note that we generally get surprisingly similar results independent of bin size. However, the particles between 1 and 8 nm radius show a greater sensitivity at the Arctic summer mesopause. For example a 14-bin model would suggest 40 particle cm^{-3} whereas the 56 and 28-bin model both agree on 10 particles cm^{-3}. In this paper we have used a 28-bin model apart from in sections 6 and 5.1 where a 14-bin model has been used.

3. General Results

[13] In this section we show results from our model as described in the previous section. As mentioned in the introduction, there are many parameters associated with meteoric smoke that are not well known. These have been set to values commonly used in 1-D studies [*Hunten et al.*, 1980; *Kalashnikova et al.*, 2000; *Gabrielli et al.*, 2004]. They include coagulation only owing to Brownian motion and sedimentation, influx of meteoric material of 44 tonnes per day and ablation primarily between 75 and 100 km. The results shown in this section thus represent a general case, which will be used as a reference case for our sensitivity studies in the coming sections.

[14] Figure 3 shows the mass distribution of meteoric material for different seasons. Throughout the year, the bulk

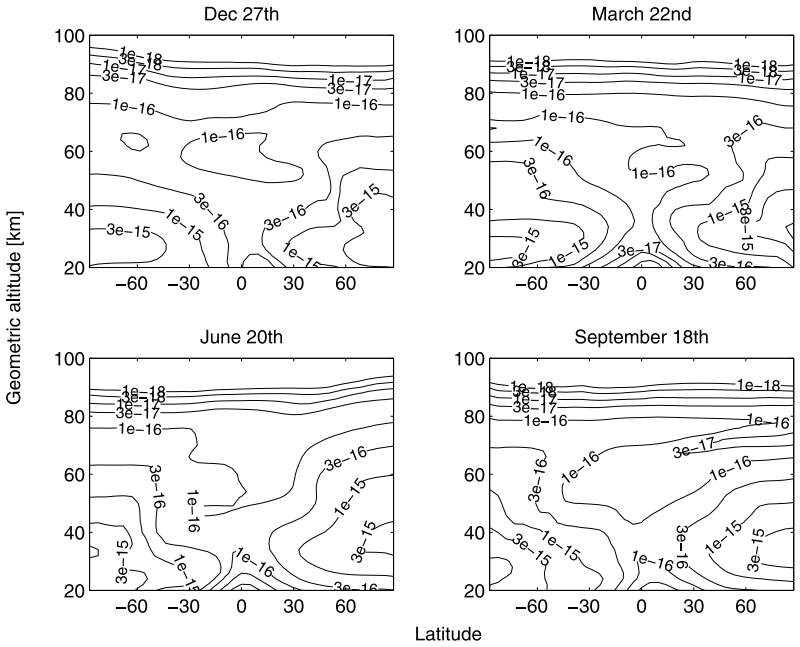

Figure 3. Global mass distribution of meteoric material in g/cm^3 for different seasons.

of the meteoric material is situated in the polar stratosphere, with the highest concentrations found during the local winter/spring. Despite the fact that the modeled ablation is independent of latitude, the mass distribution in the stratosphere varies greatly with latitude, with up to a factor 100 times more material at the poles compared to midlatitudes. This is an effect of the general atmospheric circulation, which transports material toward the winter pole and down into the polar vortex. A substantial fraction of this material remains in the stratosphere as winter turns to summer, yielding high concentrations also in the summer polar stratosphere.

[15] Figure 4 shows the total number density of particles for various times of the year. The number distribution decreases drastically with size (not shown in the figure) so that the very smallest particles, i.e., the molecular cluster sized particles, completely dominate, and the plot can be regarded as showing the distribution of these. These small particles are what prevails directly after ablation. Since ablation occurs globally, the distribution in Figure 4 is

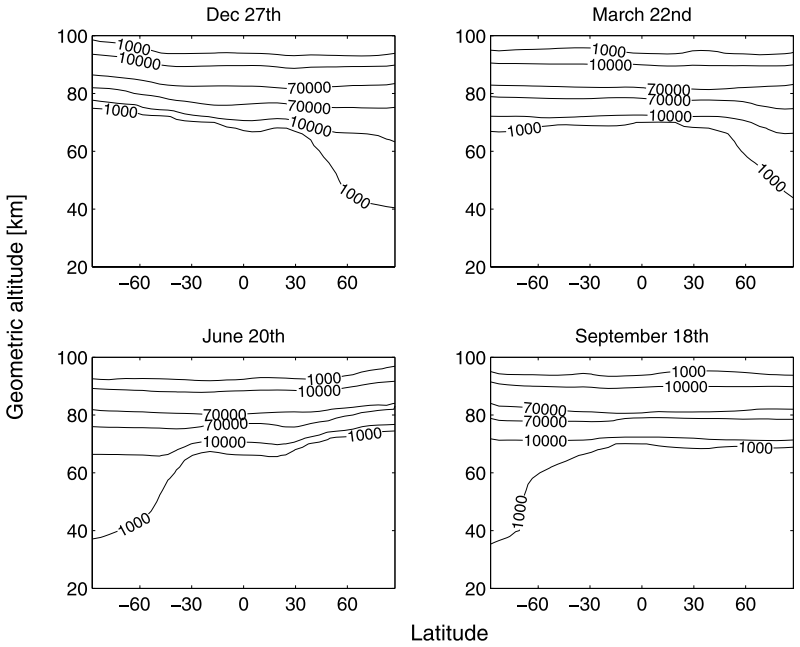

Figure 4. Global distribution of meteoric smoke for different seasons. The contours show total number density in cm^{-3}.

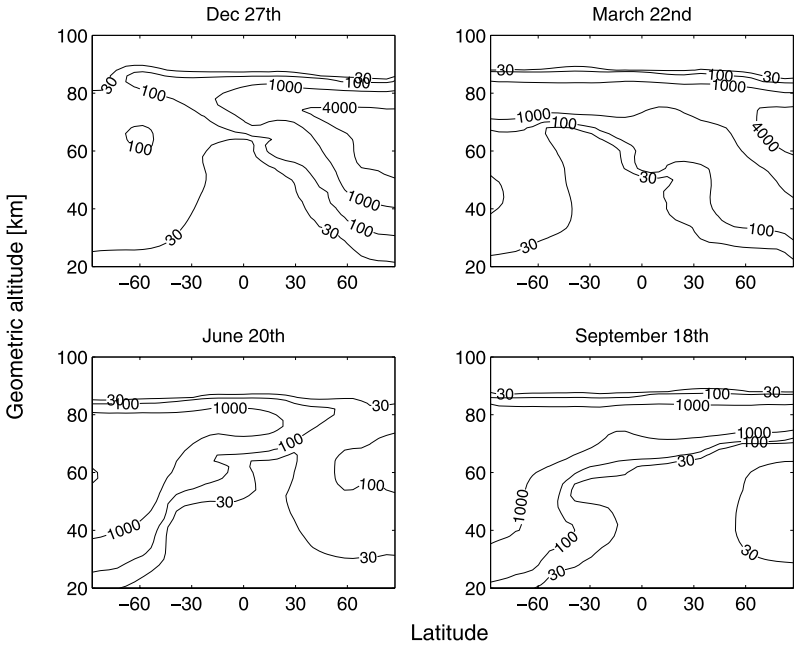

Figure 5. Global distribution of meteoric smoke for different times of the year. The contours show number density [cm^{-3}] of particles larger than 1 nm radius.

fairly steady throughout latitude and season. Nevertheless, the effect of the atmospheric circulation, which transports particles from all over the globe toward the polar winter stratosphere, is evident from the higher number densities reached near the winter pole. The maximum concentration of particles is at a slightly higher altitude at the summer pole. In our model, this is because during summer below 85 km, a given pressure surface is found at a higher altitude than in winter. This is due, in turn, to hydrostatic effects associated with the warm summer stratopause. Ultimately, the height at which ablation occurs most closely tracks pressure, since pressure in a hydrostatic atmosphere is equivalent to the integrated density column. This agrees qualitatively with experimental findings by *Lau et al.* [2006] which show a difference in meteor altitude distribution of 4 km between the summer and winter at the South Pole.

[16] The molecular cluster sized particles are too small to act as nucleation seeds for mesospheric ice phenomena. For typical mesospheric conditions a neutral particle needs to be larger than about 1 nm radius in order to serve as a condensation nucleus [*Keesee*, 1989; *Berger and von Zahn*, 2002]. The timescale to form nanometer sized particles by coagulation is long enough that these particles first appear when the material has already been transported away from the region where the ablation occurred. Hence the distribution of nanometer sized particles is very sensitive to atmospheric transport, and thus to latitude and season. In Figure 5 distributions of particles larger than 1 nm radius are shown for different seasons. The effect of atmospheric circulation, efficiently transporting the particles to the winter hemisphere, is prominent. Number densities of around 4000 cm^{-3} are reached at the winter pole, and very few particles larger than 1 nm radius remain at the polar summer mesosphere. In the beginning of the year high number densities are thus found at the north pole, and as the year proceeds, and the northern polar winter downdraft is replaced by summer updraft, a fraction of this material gets lifted up and transported to the south pole, which is now the winter pole. At the same time new material, from freshly ablated meteoroids, is fed into the system. This material is also efficiently transported to the winter pole. The result is high number densities at the north pole in December and at the south pole in June, and a more homogenous distribution in March and September when the atmospheric circulation changes direction.

[17] The low number of nanometer sized particles near the Arctic summer mesopause poses a problem. If meteoric smoke particles are the only nucleation seeds we would expect number densities of at least a few hundred cm^{-3} to explain commonly observed NLC and PMSE properties. We shall return to this in the coming sections. By comparing the two panels to the left in Figure 5, a difference between the summer solstice of the Northern and Southern Hemisphere is evident. The upper hemispheric smoke layer reaches further toward the pole in the southern summer, yielding number densities of nanometer sized particles at the summer mesopause of around 20 cm^{-3} at 68°N and 90 cm^{-3} at 68°S (exact numbers cannot be seen in figure). A more thorough study of the smoke distribution throughout the summer season (not shown in the figure) shows that the smoke concentrations reached in the southern hemispheric summer exceed those of the northern hemispheric summer. This hemispheric difference is due to stronger residual circulation in June than in December [*Siskind et al.*, 2003], which in turn is because of asymmetry in gravity wave activity between the two hemispheres.

[18] Once the particles have collected at the winter pole they continue to coagulate and sediment. The larger particles are thus found at lower altitudes in the polar winter stratosphere. As an example, the distribution of particles larger than 10 nm radius is shown in Figure 6. At altitudes

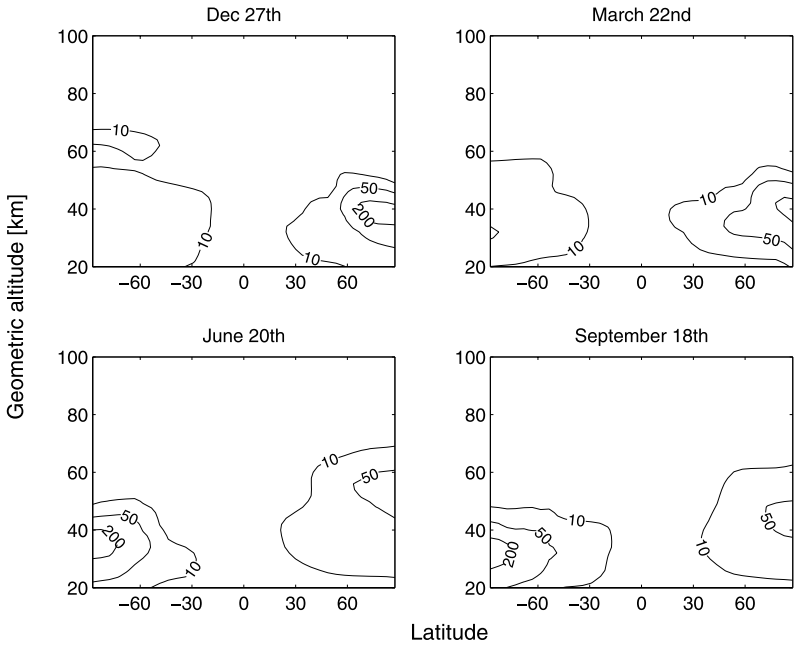

Figure 6. Global distribution of meteoric smoke for different times of the year. The contours show number density [cm^{-3}] of particles larger than 10 nm radius.

lower than 30 km the sulfuric acid rich stratospheric background aerosol, which is not included in the model, becomes important [*Vaughan and Wareing*, 2004; *Deshler et al.*, 2003]. This aerosol may react with the meteoric material, and thus alter the distribution shown in Figure 6. We note that the number density of particles larger than 10 nm exceeds 200 cm^{-3} in the winter stratosphere and 50 cm^{-3} in the summer stratosphere, which is significantly larger than the 10 cm^{-3} suggested by *Hunten et al.* [1980]. This is of course due to the middle atmospheric transport, which is not included in the Hunten et al. model, concentrating the material in the polar regions.

4. Seasonal Variation of Extraterrestrial Input

[19] The variation of the amount of ablated meteoric material with latitude and season is not completely known. Radar studies of both hemispheres show that the amount of meteors is dependent on latitude and season; at high latitudes the flux is about 3–4 times higher in the local summer/autumn than in the winter/spring, whereas the variation is less pronounced around the equator [*Singer et al.*, 2004; *Szasz et al.*, 2005; *Janches et al.*, 2006]. It is however not clear to what extent the global input of material varies throughout the year. It is also difficult to translate meteor flux data to amount of ablated meteoric material.

[20] The question of the impact of seasonal distribution of the meteoric material can be divided into the impact on the ultimate destination of the meteoric material, and the momentary impact on the local smoke distribution. As we shall see in section 6 and the former is not largely effected, whereas the local smoke distribution, in the vicinity of the ablating meteoroids, certainly is effected by variations of meteoric influx.

[21] To determine the effect on the local smoke distribution an annually varying influx at latitudes above 50° was included in the model. At low latitudes the flux was thus kept constant, whereas at high latitudes the flux was set to vary sinusoidally with 4 times more influx in the local summer/fall (September NH and February SH) than in the local winter/spring. Figure 7 shows the resulting smoke distribution of particles larger than 1 nm. By comparing these plots to Figure 5 we see that the effect of seasonal variations in extraterrestrial input on the smoke distribution is minor. A small difference is however visible at the Arctic summer mesopause where the number of nanometer-sized particles is slightly enhanced.

5. Sensitivity Study

[22] As mentioned in the introduction, many of the factors that determine the smoke particle distribution are poorly known. In this section we will investigate the impact of those factors on the smoke distribution. We will study both the effect on a population of particles above a certain size and on the total mass of meteoric material in a region. The latter is of importance for experiments that measure the absorption of light, such as occultation experiments, since in the Rayleigh limit ($r \ll \lambda$), absorption is proportional to the total volume of the particles [*van de Hulst*, 1957], or, when constant density is assumed, the total mass of the particles along the field of view. We study the mass relative to a reference case which is that described in section 3. We have chosen to focus on two locations of special importance for middle atmospheric phenomena; the Arctic summer mesopause and the Arctic winter stratosphere.

[23] The former is where noctilucent clouds form. We have selected a latitude of 68°N because this corresponds to the latitude of the radar and lidar facilities Alomar and Esrange, from which NLC often are studied. We have chosen to study the distribution at 84 km altitude, because this is just above where the clouds normally form, and thus

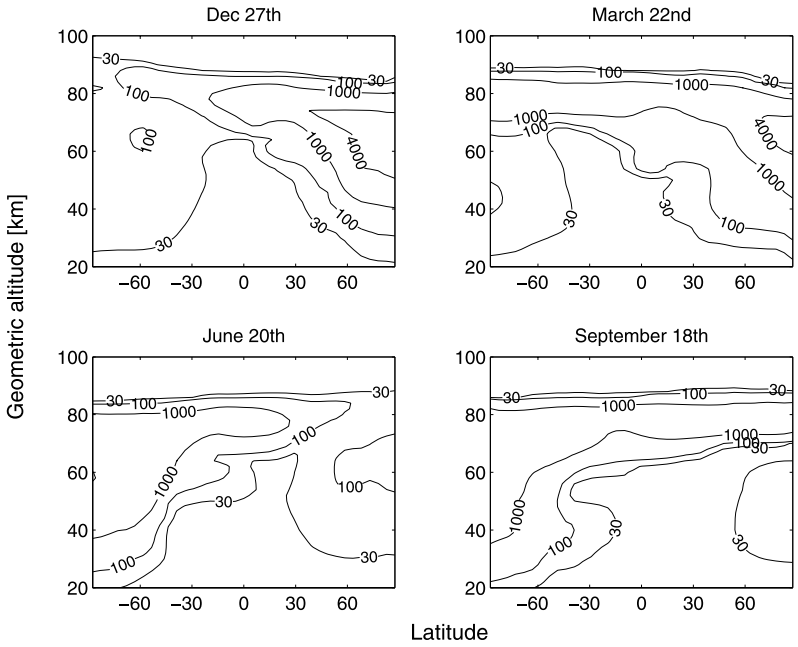

Figure 7. Global distribution of meteoric smoke for different seasons, when seasonal variation of extraterrestrial input into the atmosphere is taken into account, as described in the text. The contours show number density [cm^{-3}] of particles larger than 1 nm radius.

where nucleation seeds are needed. We study the distribution of particles larger than 1 nm radius, since this is the size typically required for a particle to act as a nucleation seed. The number density of these particles at the Arctic summer mesopause is shown as a solid line in Figures 8a, 8c, 8e, 8g, and 8i, whereas the total mass increase/decrease per cubic centimeter relative to the reference case is shown as a dashed line. The reference case is marked with a circle.

[24] The winter stratosphere is where the bulk of the material is transported to and is also of special interest because of Polar Stratospheric clouds and ozone depletion. The results are shown for an altitude of 34 km and a latitude of 90°S because this is roughly where the highest concentration of meteoric material occurs (see Figure 3) and it is above the altitude range where the sulphur species, which are not included in the model, are prominent. We choose to study the particles larger than 10 nm because this corresponds roughly to the detection limit of most measurements in this area [*Rosen and Hofmann*, 1983; *Hofmann*, 1985]. The number densities of these particles are shown as solid lines in Figures 8b, 8d, 8f, 8h, and 8j. The meteoric mass relative to the reference case is shown as a dashed lines.

5.1. Initial Size of Particles

[25] In section 3 we assumed that there is no substantial re-condensation of particles in the meteor trail because the outward diffusion of such trails is thought to be too rapid to maintain a supersaturated environment (see section 2). Hence we started our calculations with initial particle size close to molecular dimensions, i.e., a radius of 0.2 nm. To investigate the consequences if this assumption should prove to be incorrect, we have run our simulation with an initial particle size of 0.5 nm, 0.8 nm and 1.3 nm radius. These radii correspond to coalescence of 16, 64 and 270 particles of 0.2 nm radius respectively. From Figures 8a and 8b we see that neither the mass (dashed lines in Figures 8a and 8b) nor the population of 10 nm particles in the winter stratosphere (solid line in Figure 8b) is sensitive to the initial size of particle. The mesospheric population of 1 nm radius particles (solid line in Figure 8a) is fairly insensitive to the initial size of particles as long as it is no larger than 0.8 nm, i.e., the size bin below 1 nm. Note, that the model bin centered at 1.3 nm represents particles from 1.0 nm to 1.6 nm, when the 14-bin model with $V_{RAT} = 4.0$ is used. We conclude that, because of the involved time constants for particle nucleation, growth and transport, the initial radius has little influence on the final distribution. This is true as long as the initial size is significantly smaller than the size of particle we are studying. In other words, for the fate of nanometer sized smoke particles, it is not important whether or not re-condensation occurs within the meteor trail, as long as the typical particle produced by such re-condensation remains smaller than a nanometer.

5.2. Coagulation

[26] The coagulation of smoke particles in the mesosphere may be influenced by the shape, composition and the charge of the particles, out of which charge has been suggested to have a great influence [*Reid*, 1997]. Depending on the charge distribution and the resulting electrostatic forces, coagulation can both be enhanced or suppressed. The actual charge state of the particles depends on the ionospheric conditions and the particle size distribution. Our knowledge of the charging efficiency in the size range of smoke particles is limited. Particles down to sizes of a few nanometers efficiently capture charges in the form of electrons and ions [*Romay and Pui*, 1992]. Down at molecular sizes, however, charging is much less effective

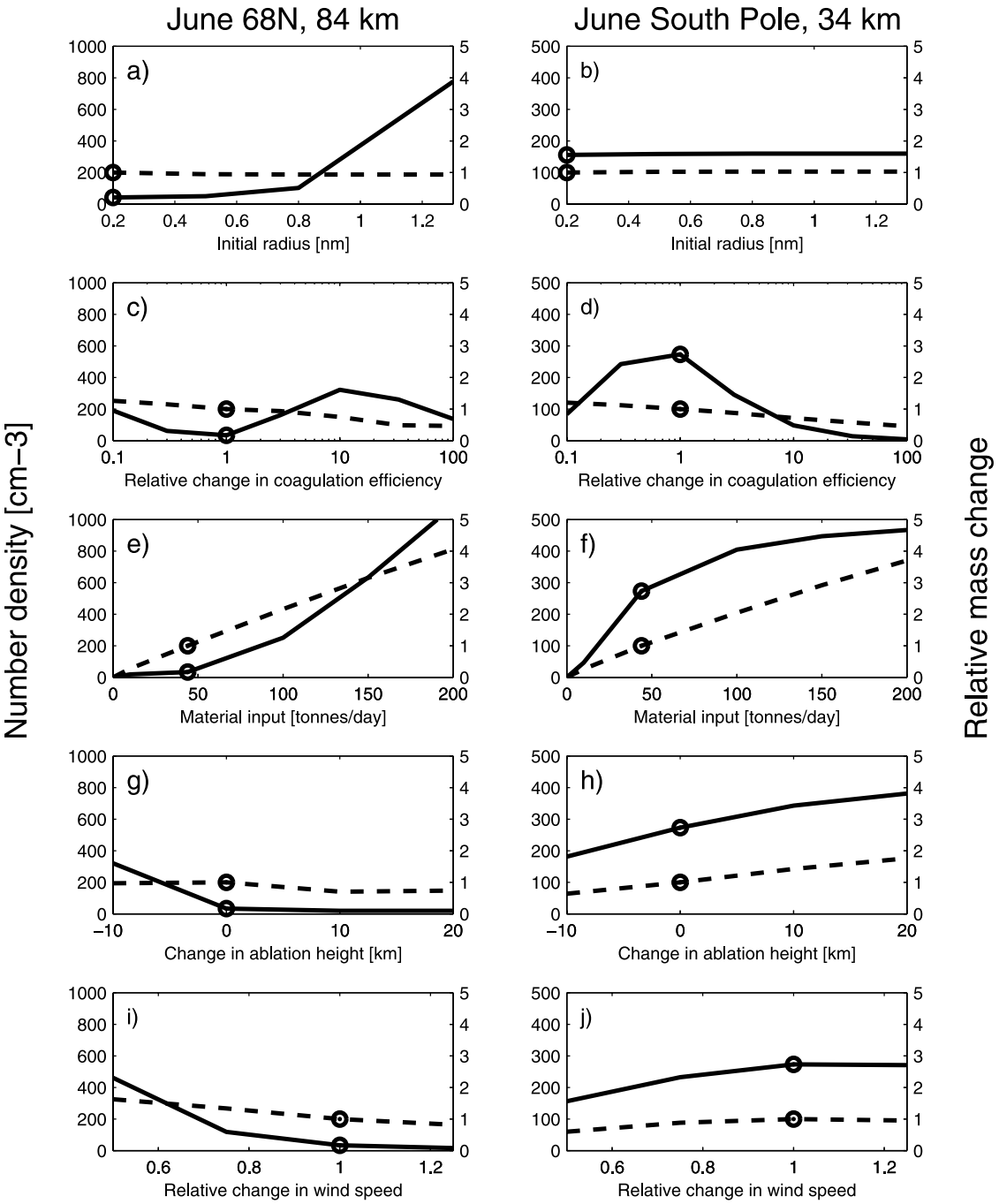

Figure 8. Effects of various factors on both the number density and mass of meteoric smoke (a, c, e, g, and i) in the Arctic summer mesopause and (b, d, f, h, and j) in the Arctic winter stratosphere. The dashed lines show the variation of the mass of meteoric material relative to our reference case described in section 3 and should be read out on the right-hand axes. A factor 2 on the right-hand axis means that the mass of meteoric material in the particular region is doubled compared to what is shown in Figure 3. The solid lines in Figures 8a, 8c, 8e, 8g, and 8i give the number density of particles larger than 1 nm radius at the Arctic summer mesopause, i.e., the population of possible nucleation kernels for NLC and PMSE. The solid lines in Figures 8b, 8d, 8f, 8h, and 8j show the population of particles larger than 10 nm at the Arctic winter stratosphere. Both should be read out on the left-hand axes in units of cm^{-3}. In all plots the reference case is marked with a circle. Figures 8a and 8b thus show the effect of the initial particle size on the smoke distribution in the Arctic summer mesopause and the winter polar stratosphere. In the same way, Figures 8c and 8d show the effect of a factor 0.1 to 100 change in coagulation efficiency; Figures 8e and 8f show the response to amount of extraterrestrial material input to the atmosphere; Figures 8g and 8h show the effect of shifting the ablation profile 10 km down and 20 km up; and Figures 8i and 8j show the effect of altered residual circulation by factors ranging from 0.5 to 1.5.

and governed by the electronegativity and the chemical properties of molecules. Little is today known about the transition between these two regimes, i.e., the charging of smoke particles between molecular size and nanometer size. It is unlikely that a majority of subnanometer smoke particles is charged in the mesosphere. Considering the large number of these particles, such a charging would lead to persistent large-scale depletions of electron (and ion) concentrations in the D region, which is generally not observed.

[27] Under typical conditions in the ionospheric D region, a fraction of the smoke particles is expected to charge negatively since mobile electrons are more readily captured than heavier ions [*Rapp and Lübken*, 2001]. The coagulation of particles carrying the same charge sign is then strongly reduced by electrostatic repulsion. This leads to a reduction of the coagulation efficiency that is essentially proportional to the fraction of charged particles. At the same time, coagulation between charged and neutral particles is enhanced by induced dipole interaction. However, under ionospheric conditions with very low ionization rates, it is possible that charge capture by particles leads to depletions of both electrons and ions [*Rapp and Lübken*, 2001]. In this case, both positive and negative particles will be present, thus substantially enhancing the coagulation efficiency by electrostatic attraction. It can be noted, however, that this case is unlikely particularly in the polar summer mesosphere where ionization rates are high due to permanently sunlit conditions and frequent energetic particle precipitation. In order to test the influence of both decreased and enhanced coagulation efficiency owing to charging, we have performed a sensitivity study decreasing or increasing the coagulation kernels by factors between 0.1 and 100.

[28] The solid line in Figure 8c shows how the number of nanometer sized particles at the Arctic summer mesopause varies with coagulation efficiency. It is interesting to note that both an increase and a reduction of the coagulation efficiency with a factor 10 increases the number of nanometer sized particles at the summer mesopause to 200–300 cm^{-3}. An increase of the coagulation efficiency causes more of the freshly ablated material to grow to nanometer sized particles before it is transported away. A reduction of the coagulation efficiency, however, results in higher numbers of nanometer sized particles in the stratosphere, which can be brought back to the mesosphere by the summer updraft circulation. An increase of the coagulation efficiency by more than a factor 10 does however not result in a further increase of particles. Instead the particles grow so large that they sediment out of the region.

[29] Even though the coagulation efficiency may influence the number densities and the size distribution of the particles drastically, it has little effect on the mass distribution. This is not surprising, since total mass is invariant under coagulation. However, a small decrease with increasing coagulation efficiency is to be expected because of the increase in sedimentation speed associated with larger particles. The dashed line in Figure 8c shows that the effect on the meteoric mass at the Arctic summer mesopause is less than a factor 2. This is however minor compared to the large variations in mass distribution with latitude and height shown in Figure 3.

[30] In the winter stratosphere, increased coagulation means more sedimentation both down into and out of the stratosphere. The net result is a small decrease in mass as shown by the dashed line in Figure 8d. The population of particles larger than 10 nm decreases both with increased and decreased coagulation efficiency. This is due to the competition between more efficient coagulation to 10 nm and faster sedimentation and coagulation to even bigger particles.

5.3. Amount of Meteoric Material

[31] The estimates of how much meteoric material enters Earth's atmosphere range from 5 to 400 tonnes per day [*Gabrielli et al.*, 2004; *Love and Brownlee*, 1993; *Mathews et al.*, 2001; *Ceplecha et al.*, 1998]. However, for atmospheric studies, it is enough to consider the particle mass range between 10^{-7}g and 10^{-3}g [*von Zahn*, 2005]. Smaller particles than this do not ablate and bigger impacts are very rare and the involved meteoroids do not fully ablate. Part of this range may thus be explained by the sensitivity to different mass ranges of the various techniques.

[32] Figure 8e shows the sensitivity to a meteoric mass input between 10 and 200 tonnes per day. Not surprisingly this has a drastic effect on both the mass and the population of nanometer sized particles in the Arctic summer mesopause. The mass that is resident in this part of the atmosphere is proportional to the amount of input (dashed line). The number of nanometer sized particles (solid line) show an even greater sensitivity to the mass influx, because coagulation to nanometer sized particles is favored by a greater mass of ablated material. This makes number densities of up to 1000 cm^{-3} near the polar summer mesopause possible.

[33] In the Arctic winter stratosphere the mass is still proportional to the amount of extraterrestrial input (dashed line in Figure 8f), but the 10 nm particle population is less sensitive. The reason is the more rapid coagulation to larger particles, which leads to higher sedimentation out of the region.

5.4. Height of Ablation

[34] The altitude at which a meteoroid ablates is determined by its velocity and impact angle, so that a faster meteoroid owing to a more rapid deceleration will ablate higher up than an identical, but slower, meteoroid. Since the mean velocity, with which the meteoroids enter the atmosphere, is not well known [*Janches and Mathews*, 2000], this results in an uncertainty of the ablation altitude [*Hunten et al.*, 1980]. In our reference case the ablation takes place mainly between 75 and 100 km, but significant ablation can occur up to an altitude of 120 km [*Plane*, 2004; *Janches and ReVelle*, 2005]. Here we have studied the effects of shifting the ablation profile, which peaks at 84 km, both 10 km downward and 20 km upward. The effects can be seen in Figures 8g and 8h. The smoke distribution is in general not very sensitive to the height of ablation as long as it not below the strong meridional winds at 80–90 km. Ablation below this means that it takes longer time for the material to be transported away from its original location, resulting in a greater number of nanometer sized particles at the Arctic summer mesopause, as can be seen by the solid line in Figure 8g. Not surprisingly, the Arctic winter stratosphere receives more material if all of the ablation occurs above the

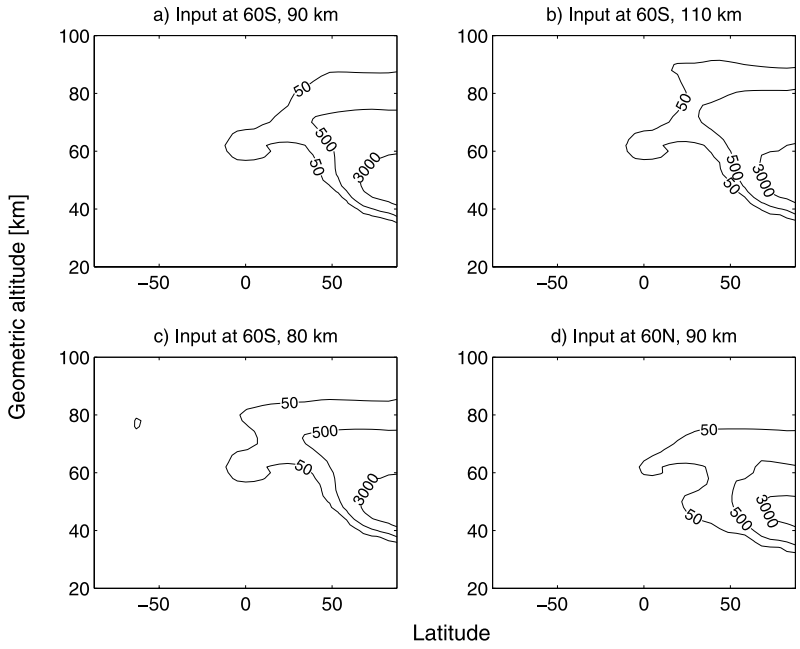

Figure 9. Total number concentration in cm^{-3} 45 days after input of a test cloud distribution at various locations.

main meridional transport, the effect on both the mass and the particle distribution is however less than a factor 2 (Figure 8h).

5.5. Meridional Circulation

[35] Our results for dust transport will only be as accurate as the mean meridional circulation simulated by CHEM2D. In turn, the mean meridional circulation is tuned to match various temperature climatologies as discussed by *Siskind et al.* [2003, 2005]. The primary mechanism for tuning the circulation is the gravity wave drag model: wave amplitudes, launch altitude, phase spectrum and intensity at each phase speed. While the resulting temperatures are in good agreement with observations, we must acknowledge the possibility that this agreement results from a nonunique solution for the meridional circulation. Even if the model wind field, as mentioned earlier, agrees well with several established models ([*Sassi et al.*, 2004; *Becker and Fritts*, 2006; *McLandress et al.*, 2006]), *Siskind et al.* [2003] mentioned that their meridional jet differs in some ways to that derived semi-empirically from HRDI observations by *Lieberman et al.* [2000]. Specifically between 80 and 90 km, the *Lieberman et al.* [2000] winds were about a factor of two weaker than CHEM2D. This may be of importance because the timescale for dust transport depends upon the meridional wind at the altitude of maximum ablation. In our calculation, the meridional jet maximum and the ablation altitudes largely coincide. Earlier we have shown that the altitude of ablation is unimportant as long as it is above the meridional jet. If however, the actual meridional wind were that of *Lieberman et al.* [2000], the timescale for transport to the winter pole would be 2 times less. In order to evaluate how this would effect the dust distribution, the wind field of our model was simply reduced up to a factor 2. We note that a reduced wind field, or a wind field where the meridional circulation has its maximum below the main ablation, is one way that could provide for higher number densities of nanometer sized particles at the summer mesopause, up to 500 cm^{-3} (Figure 8i). At the same time this would reduce the amount of material collected at the winter stratosphere (Figure 8j).

6. Transport Timescales

[36] We have seen that the bulk of the meteoric material is transported to the Arctic winter stratosphere. In this section we investigate how robust this result is. To do this the continuous input of freshly ablated material was removed and was replaced by a "test cloud" of smoke particles entered at various heights, latitudes and times of the year. The evolution of these particles as they coagulate and get transported is then studied. This is obviously not representative for the way the meteoric material is deposited in the atmosphere, but provides a straight forward way of understanding the timescales involved in transport and coagulation. Moreover, it offers a simple way to determine the impact of factors such as the ablation height and seasonal variations of material input. The test cloud consists of 0.2 nm radius particles with number densities (N) described by a Gaussian distribution in altitude and latitude according to

$$N = A \times \frac{1}{\sigma_z\sqrt{2\pi}} \times e^{\frac{(z-\mu_z)^2}{2\sigma_z^2}} \times \frac{1}{\sigma_\phi\sqrt{2\pi}} \times e^{\frac{(\phi-\mu_\phi)^2}{2\sigma_\phi^2}} \quad (2)$$

where $A = 10^5$ particles cm^{-3} is the peak number density, z and ϕ are the vertical and latitudinal coordinates respectively, μ_z and μ_ϕ the mean of the distributions in these coordinates and σ_z, σ_ϕ the standard deviations in the same coordinates (both set to 5 km). It was found that the time required for such a test cloud to move from the equator to the pole was about 20 days. Figure 9a displays the result of a test cloud entered at $\mu_z = 90$ km and $\phi_z = 60°$S in January. The figure shows the distribution of particles 45 days after

the cloud was entered. The particles have accumulated in the winter stratosphere. We now compare the result of this reference cloud to test clouds entered at other locations in order to study the sensitivity to height of ablation as well as to latitudinal position of meteoroid entrance. Figures 9b–9d show the results for test clouds entered at (μ_z = 110 km, ϕ_z = 60°S), (μ_z = 80 km, ϕ_z = 60°S) and (μ_z = 90 km, ϕ_z = 60°N). The distributions are remarkably similar. The distribution resulting from the test cloud entered at ϕ_z = 60°N, i.e., in the winter hemisphere, (Figure 9d) is located at a slightly lower altitude. This is simply because the cloud is closer to the winter polar vortex and reaches it faster. Hence it has more time to move down into the vortex. Concerning the ultimate destination of the meteoric material, we thus conclude that the effects of ablation height, and latitudinal dependence of the meteoric input are both small, as long as the ablation occurs at or above the altitude range of strong meridional summer to winter transport. As we have seen in the previous section, ablation below the strong meridional winds does indeed have an effect on the particle distribution.

[37] Temporal effects of the meteor flux were investigated by entering the test cloud in June instead of January (not shown in the figure), at the same position as our reference cloud. Naturally, in this case, the opposite direction of the atmospheric circulation transports the cloud of particles to the current winter pole; the south pole. The distribution is therefore more or less the mirror image of our reference cloud result. For the ultimate fate of the meteoric material, the hemispheric seasonal variations of the meteoric input are only important if there is an annual variation of global input. For instance, if the whole earth would receive more meteoric material during January, this would result in more material collected at the north pole than at the south pole. However, if the variations on the two hemispheres cancel each other, so that the global input is roughly constant, the annual collection of meteoric material in both hemispheres should be of similar magnitudes. Currently, it is not fully understood to which degree this cancellation occurs.

7. Discussion

[38] We have here presented the first 2-D model study of microphysics and transport of meteoric smoke particles in the middle atmosphere. We have shown that it is possible to satisfactorily model the coagulation process of smoke particles with significantly less radius size bins than previous 1-D studies have used. The reduced computation time achieved with less bins opens up the possibility for 3-D studies of similar topics.

[39] The general circulation of the mesosphere, an updraft at the summer pole, transport toward the winter pole and a downdraft over the winter pole, has been shown to effectively transport meteoric material to the winter stratosphere. The timescale of transport from equator to polar regions is obviously dependent on the wind field, and thus the altitude, but is typically around 20 days. The effect of the transport is not so apparent on the very smallest, short-lived smoke particles, smaller than 1 nm radius, which are produced in situ by meteoric ablation. However, the effect on the nanometer sized smoke distribution is drastic. This is due to the timescale (∼days) at which nanometer sized particles form by coagulation. During this time the material is transported toward the winter hemisphere, with a typical transport velocity of 3–5° per day. Hence the nanometer sized particles first appear when the air parcel has been transported away from its original position. The result is a distribution of nanometer sized smoke which is very dependent on latitude and season. This contrasts with the simplistic picture of a homogeneous global meteoric smoke layer, which is currently assumed in many studies of middle atmospheric phenomena, such as noctilucent clouds and PMSEs. It is therefore crucial to take the global transport of smoke particles into account when modeling these phenomena.

[40] Using the same coagulation rate, influx of meteoric material and ablation height as commonly has been used in 1-D studies [*Hunten et al.*, 1980; *Gabrielli et al.*, 2004], results in less than 100 nanometer sized smoke particles cm^{-3} in the Arctic summer mesopause, where they are believed to serve as nucleation seeds for NLCs and PMSEs. If smoke particles are the only nucleation kernel this would imply less than 100 ice particles per cubic centimeter at the summer mesopause. This is peculiar, since middle atmospheric ice phenomena (NLC and PMSE) are believed to consist of much higher ice number densities. However, as we have seen, the number of nucleation kernels is sensitive to many factors that are poorly known. Such factor include the amount of extraterrestrial material that gets deposited in Earth's atmosphere, the coagulation efficiency, which in turn is dependent on shape, composition and charge of the particles, and the strength of the meridional circulation. Considering the total uncertainty range of these factors may number densities up to a few hundred or a thousand may become feasible. This is closer to what is expected for mesospheric ice phenomena. Other factors, however, have been shown to have surprisingly little effect on the smoke distribution. These include the initial size of particles, i.e., the size of the particles that are produced in the meteoric ablation, the seasonal variations of meteoric input and the height of meteoric ablation as long as it is above or around the maximum of the meridional wind field. It is also worth noting that the mass of meteoric material at the Arctic summer mesopause is remarkably stable with regards to all the poorly known factors, apart from the extraterrestrial input, with which it is linear. Detection of smoke layers by light absorption techniques, which see the total volume, or, assuming constant density, the total mass along the field of view, should thus be rather insensitive to these factors.

[41] Measurements of nanometer sized particles in the mesosphere suffer, as pointed out in the introduction, from aerodynamical issues preventing smaller particles from reaching the detector. This leads to a size cutoff, which varies greatly with altitude, and is difficult to estimate. The modeled size distribution in the mesosphere increases drastically with decreasing radius, making predicted number densities of particles extremely sensitive to the size cutoff. Another problem is that measurements thus far are only available for the charged fraction of the total particle population, which depends on generally unknown local ionospheric conditions. A direct comparison of our model results to available data is therefore in principle only possible if both the aerodynamical and instrumental size cutoffs, as well as the charged fraction of the total particle population, are known. Unfortunately, there are no measurements available, for which all these quantities have been determined.

[42] A measurement that has taken aerodynamics into account when considering the sensitivity of their detector has been reported by *Rapp et al.* [2005] who launched a rocket from Esrange (68°N) in October 2004. They detected positively charged particles of number densities reaching 100 cm^{-3} at an altitude of 86 km. At this altitude their aerodynamical calculations suggested a minimal detectable radius of ~2 nm [*Hedin et al.*, 2007]. For the corresponding position and season our model suggests ~10 particles cm^{-3} larger than 2 nm, i.e., lower than what is measured. However, if the true size cutoff was only slightly lower than what they suggest, 1.5 nm, the exponential increase in modeled particle brings the expected number up to 100 cm^{-3}. This example proves the importance of determining the aerodynamical size cutoff with as high precision as possible. It is also worth noting, that if the local ablation takes place only 10 km higher than our average model ablation profile, i.e., more in line with what recent calculations suggest [*Janches and ReVelle*, 2005], number densities of 2 nm particles of 100 cm^{-3} are reached at the location of the measurements. Given the uncertainties involved, a factor 10 difference between the measured and modeled number of particles must thus be considered reasonable.

[43] The lack of knowledge of the lower size cutoff from other experiments makes comparisons with our results meaningless. However, it is interesting to note that all the experiments specifically aimed at measuring mesospheric particles in the absence of NLC/PMSE have detected positively charged [*Gelinas et al.*, 1998] or negatively charged particles [*Lynch et al.*, 2005] of number densities ranging from a few particles cm^{-3} to a few 100 particles cm^{-3}. These numbers fit well with our results for nanometer sized particles.

[44] If the aerodynamics is not properly understood and accounted for, it is only possible to draw conclusions about the relative differences between measurements where identical instruments have been used and where the rocket velocities through the region of measurements have been the same. Unfortunately, there are currently no such sets of measurements which have been conducted at different latitudes or at different seasons. The seasonal and latitudinal variations suggested by our model are therefore not possible to verify with the available experimental data. In order to be able to do meaningful comparisons of theory and data, experiments for which the aerodynamics can be understood and the size detection limit can be determined, are thus of great importance. Moreover, measurements of the total (neutral + charged) particle distribution and measurements at different seasons and latitudes are necessary to understand the distribution and transport of the extraterrestrial material.

[45] Our model shows that larger particles collect at the Arctic stratosphere. The number densities of particles larger than 10 nm radius reach ~300 cm^{-3} at winter stratosphere and 50 cm^{-3} at the summer stratosphere, which is significantly larger than the 10 cm^{-3} suggested by *Hunten et al.* [1980]. The winter population is rather stable with regards to the studied poorly known factors, and in most scenarios show number densities between 100 and 500 cm^{-3}. In a similar way to the situation in the mesosphere, we found that the ambient mass in the stratosphere is remarkably independent of these poorly known factors, apart from the amount of meteoric input. These high predicted concentrations of meteoric smoke particles in the polar stratosphere may be of importance for stratospheric nucleation processes and for the formation of Polar Stratospheric Clouds (PSC). *Voigt et al.* [2004] find that their observations of PSC cannot be explained neither by homogeneous Nitric Acid Trihydrate (NAT) nucleation nor by NAT nucleation on ice. They therefore consider meteoric smoke particles the "favorable candidates for triggering NAT nucleation."

[46] Our results concerning transport of dust into the stratosphere are consistent with several experimental findings. *Curtius et al.* [2005] have measured the fraction of nonvolatile particles in the Arctic lower stratosphere. They conclude that "the fraction of meteoric material in stratospheric particles at similar altitudes is distinctly higher inside the Arctic vortex compared to outside." Measurements of iridium and platinum, which to a large extent have an extraterrestrial origin, in Greenland ice cores [*Gabrielli et al.*, 2004], yield higher concentrations of meteoric material than expected from a globally uniform distribution. The authors argue that the reason behind this higher concentration is a focusing effect produced by the meridional circulations, which is just what our model shows.

[47] Our modeled number densities of particles are consistent with stratospheric balloon measurements of the so-called CN (Condensation Nuclei) layer. This is a layer of small (10–100 nm) particles with much higher number densities than the usual stratospheric background aerosol layer [*Deshler et al.*, 2003; *Rosen and Hofmann*, 1983; *Hofmann*, 1985]. Several explanations for the CN layer have been proposed, such as downward transport of SO_2 followed by local production of H_2SO_4 vapor which then form particles through heterogeneous nucleation [*Vaida et al.*, 2003]. Meteoric smoke has been suggested as a possible explanation but disregarded on the basis of the low concentrations of meteoric particles suggested by 1-D models [*Zhao et al.*, 1995]. The measured number densities of the CN layer are generally between 1 and 10 cm^{-3} [*Deshler et al.*, 2003] but enhanced concentrations of a few 100 cm^{-3} have been measured on several occasions in the polar regions during the winter/spring [*Rosen and Hofmann*, 1983; *Hofmann*, 1985]. These concentrations are very much in agreement with our new model estimates for particles of the same size range (10–100 nm). The significance of smoke for the CN layer should thus be reconsidered.

8. Conclusions

[48] This first 2-D study of meteoric smoke predicts that the middle atmospheric circulation is of major importance for the smoke distribution, as it efficiently transports the meteoric material to the winter stratosphere. The distribution of nanometer sized smoke particles thus becomes highly dependent on latitude and season. Commonly used 1-D meteoric smoke profiles, such as the one from the ground-breaking work by *Hunten et al.* [1980], refer to average global conditions, which are very different from the local situation in the real atmosphere. These 1-D profiles should therefore not be used in studies of latitudinal dependent middle atmospheric phenomena.

[49] Using similar assumptions about meteoric influx, ablation height and coagulation efficiency as commonly

used in 1-D studies [*Hunten Et kal.*, 1980; *Kalashnikova et al.*, 2000; *Gabrielli et al.*, 2004] results in less than 100 nanometer sized smoke particles cm^{-3} at the polar summer mesopause and around 300 particles cm^{-3} larger than 10 nm at the winter stratosphere. This can be compared with the results of 1-D models, which suggest of the order of a thousand nanometer sized particles cm^{-3} at the summer mesopause and around 10 particles cm^{-3} larger than 10 nm in the winter stratosphere. Conclusions based on the numbers given by 1-D models, such as ice nucleation on smoke in the Arctic summer mesosphere and the significance of smoke for middle stratospheric CN layer, should thus be re-evaluated.

[50] However, the limited knowledge of the basic parameters that determine the smoke formation, such as composition, charge, shape of the particles and influx of extraterrestrial material imposes considerable uncertainties on the smoke distribution. Whereas the total mass resident in the winter stratosphere is rather insensitive to these factors, the number densities of nanometer sized smoke particles at the Arctic summer mesopause show a great sensitivity, possibly allowing for concentrations of condensation nuclei more in line with those expected for mesospheric ice phenomena. Measurements of the composition and charged fraction of smoke particles, as well as measurements with controlled aerodynamics conducted at different latitudes and seasons, are therefore of great importance to fully understand the role of meteoric smoke in the middle atmosphere.

[51] **Acknowledgments.** The authors thank the National Center of Atmospheric Research for providing on-line data from the Whole-Atmosphere Community Climate Model (WACCM). L. Megner thanks Csilla Szasz and Johan Kero at the Swedish Institute of Space Physics and Heiner Körnich at Stockholm University for helpful discussions. This project was supported by the Swedish National Space Board. D. E. Siskind's time was funded by the Office of Naval Research and the NASA Living With a Star program. M. Rapp was supported by the Deutsche Forschungsgemeinschaft under grant RA 1400/2-1.

References

Bailey, S. M., A. W. Merkel, G. E. Thomas, and J. N. Carstens (2005), Observations of polar mesospheric clouds by the Student Nitric Oxide Explorer, *J. Geophys. Res.*, *110*, D13203, doi:10.1029/2004JD005422.

Becker, E., and D. C. Fritts (2006), Enhanced gravity-wave activity and interhemispheric coupling during the MacWAVE/MIDAS northern summer program 2002, *Ann. Geophys.*, *24*, 1175–1188.

Berger, U., and U. von Zahn (2002), Icy particles in the summer mesopause region: Three-dimensional modeling of their environment and two-dimensional modeling of their transport, *J. Geophys. Res.*, *107*(A11), 1366, doi:10.1029/2001JA000316.

Ceplecha, Z., J. Borovicka, W. G. Elford, D. O. Revelle, R. L. Hawkes, V. Porubcan, and M. Simek (1998), Meteor phenomena and bodies, *Space Sci. Rev.*, *84*, 327–471.

Colela, P., and P. R. Woodard (1984), The piecewise parabolic method (PPM) for gas-dynamical simulations, *J. Comput. Phys.*, *54*, 174–201.

Croskey, C., J. Mitchell, M. Friedrich, K. Torkar, U.-P. Hoppe, and R. Goldberg (2001), Electrical structure of PMSE and NLC regions during the DROPPS program, *Geophys. Res. Lett.*, *28*, 1427–1430.

Curtius, J., et al. (2005), Observations of meteoritic material and implications for aerosol nucleation in the winter arctic lower stratosphere derived from in situ particle measurements, *Atmos. Chem. Phys.*, *5*, 5039–5080.

Deshler, T., M. E. Hervig, D. J. Hofmann, J. M. Rosen, and J. B. Liley (2003), Thirty years of in situ stratospheric aerosol size distribution measurements from Laramie, Wyoming (41°N), using balloon-borne instruments, *J. Geophys. Res.*, *108*(D5), 4167, doi:10.1029/2002JD002514.

Fiocco, G., and G. Grams (1971), On the origin of noctilucent clouds: Extraterrestrial dust and trapped water molecules, *J. Atmos. Terr. Phys.*, *33*, 815–824.

Gabrielli, P., et al. (2004), Meteoric smoke fallout over the holocene epoch revealed by iridium and platinum in Greenland ice, *Nature*, *432*, 1011–1014.

Gelinas, L. J., K. A. Lynch, M. C. Kelley, S. Collins, S. Baker, Q. Zhou, and J. S. Friedman (1998), First observation of meteoritic charged dust in the tropical mesosphere, *Geophys. Res. Lett.*, *25*, 4047–4050.

Gumbel, J. (2005), The magic rocket campaign—An overview, *Eur. Space Agency, Spec. Publ.*, *590*, 139–144.

Hedin, J., J. Gumbel, and M. Rapp (2007), On the efficiency of rocket-borne particle detection in the mesosphere, *Atmos. Chem. Phys. Discuss.*, *7*, 1183–1214.

Hervig, M., and D. E. Siskind (2006), Decadal and inter-hemispheric variability in polar mesospheric clouds, water vapor, and temperature, *J. Atmos. Sol. Terr. Phys.*, *680*, 30–41.

Hofmann, D. J. (1985), Antarctic observations of stratospheric aerosols and high altitude condensation nuclei following the El Chichon eruption, *Geophys. Res. Lett.*, *12*, 13–16.

Horanyi, M., J. Gumbel, G. Witt, and S. Robertson (1999), Simulation of rocket-borne particle measurements in the mesosphere, *Geophys. Res. Lett.*, *26*, 1537–1540.

Hunten, D. M., R. P. Turco, and O. B. Toon (1980), Smoke and dust particles of meteoric origin in the mesosphere and stratosphere, *J. Atmos. Sci.*, *37*, 1342–1357.

Jacobson, M. Z., R. Lu, E. J. Jensen, and O. B. Toon (1994), Modelling coagulation among particles of different composition and size, *Atmos. Environ.*, *28*, 1327–1338.

Janches, D., and J. D. Mathews (2000), Micrometeor observations using the Arecibo 430 MHz radar. i. determination of the ballistic parameter from measured Doppler velocity and deceleration results, *Icarus*, *145*, 53–63.

Janches, D., and D. O. ReVelle (2005), Initial altitude of the micrometeor phenomenon: Comparison between Arecibo radar observations and theory, *J. Geophys. Res.*, *110*, A08307, doi:10.1029/2005JA011022.

Janches, D., C. J. Heinselman, J. L. Chau, A. Chandran, and R. Woodman (2006), Modeling the global micrometeor input function in the upper atmosphere observed by high power and large aperture radars, *J. Geophys. Res.*, *111*, A07317, doi:10.1029/2006JA011628.

Jensen, E. J., O. B. Toon, S. A. Vay, J. Ovarlez, R. May, T. P. Bui, C. H. Twohy, B. W. Gandrud, and R. F.P. U. Schumann (2001), Prevalence of ice-supersaturated regions in the upper troposphere: Implications for optically thin ice cloud formation, *J. Geophys. Res.*, *106*, 17,253–17,266.

Kalashnikova, O., M. Hornayi, G. E. Thomas, and O. B. Toon (2000), Meteoric smoke production in the atmosphere, *Geophys. Res. Lett.*, *27*, 3293–3296.

Keesee, R. G. (1989), Nucleation and particle formation in the upper atmosphere, *J. Geophys. Res.*, *94*, 14,683–14,692.

Kornblum, J. J. (1970), Collection efficiency for inertial impaction and sounding rocket collection of meteoric dust, *J. Geophys. Res.*, *75*, 3976–3986.

Lau, E. M., S. K. Avery, J. P. Avery, D. Janches, S. E. Palo, R. Schafer, and N. A. Makarov (2006), Statistical characterization of the meteor trail distribution at the South Pole as seen by a VHF interferometric meteor radar, *Radio Sci.*, *41*, RS4007, doi:10.1029/2005RS003247.

Lieberman, R. S., et al. (2000), Comparison of mesospheric and lower thermospheric residual wind with High Resolution Doppler Imager, medium frequency, and meteor radar winds, *J. Geophys. Res.*, *105*, 27,023–27,036.

Love, S. G., and D. E. Brownlee (1993), A direct measurement of the terrestrial mass accretion rate of cosmic dust, *Science*, *262*, 550–553.

Lynch, K. A., L. J. Gelinas, M. C. Kelley, R. L. Collins, M. Widholm, D. Rau, E. MacDonald, Y. Liu, J. Ulwick, and P. Mace (2005), Multiple sounding rocket observations of charged dust in the polar winter mesosphere, *J. Geophys. Res.*, *110*, A03302, doi:10.1029/2004JA010502.

Mathews, J. D., D. Janches, D. D. Meisel, and Q. H. Zhou (2001), The micrometeoroid mass flux into the upper atmosphere: Arecibo results and comparision with prior estimates, *Geophys. Res. Lett.*, *28*, 1929–1932.

McLandress, C., W. E. Ward, V. I. Fomichev, K. Semeniuk, S. R. Beagley, N. A. McFarlane, and T. G. Shepherd (2006), Large-scale dynamics of the mesosphere and lower thermosphere: An analysis using the extended Canadian Middle Atmosphere Model, *J. Geophys. Res.*, *111*, D17111, doi:10.1029/2005JD006776.

Megner, L., M. Rapp, and J. Gumbel (2006), Distribution of meteoric smoke—Sensitivity to microphysical properties and atmospheric conditions, *Atmos. Chem. Phys.*, *6*, 4415–4426.

Plane, J. M. C. (2000), The role of sodium bicarbonate in the nucleation of noctilucent clouds, *Ann. Geophys.*, *18*, 807–814.

Plane, J. M. C. (2004), A time-resolved model of the mesospheric na layer: Constraints on the meteor input function, *Atmos. Chem. Phys.*, *4*, 627–638.

Rapp, M., and F.-J. Lübken (2001), Modelling of particle charging in the polar summer mesosphere: Part 1—General results, *J. Atmos. Sol. Terr. Phys.*, *63*, 759–770.

Rapp, M., and G. E. Thomas (2006), Modeling the microphysics of mesospheric ice particles—Assessment of current capabilities and basic sensitivities, *J. Atmos. Sol. Terr. Phys.*, *68*, 715–744.

Rapp, M., J. Hedin, I. Strelnikova, M. Friedrich, J. Gumbel, and F.-J. Lbken (2005), Observations of positively charged nanoparticles in the nighttime polar mesosphere, *Geophys. Res. Lett.*, *32*, L23821, doi:10.1029/2005GL024676.

Reid, G. C. (1975), Ice clouds at the summer polar mesopause, *J. Atmos. Sci.*, *32*, 523–535.

Reid, G. C. (1997), On the influence of electrostatic charging on coagulation of dust and ice particles in the upper mesosphere, *Geophys. Res. Lett.*, *24*, 1095–1098.

Romay, F. J., and D. Y. H. Pui (1992), Free electron charging of ultrafine aerosol particles, *J. Aerosol Sci.*, *23*, 679–692.

Rosen, J. M., and D. J. Hofmann (1983), Unusual behavior in the condensation nuclei concentration at 30 km, *J. Geophys. Res.*, *88*, 3725–3731.

Rosinski, J., and R. H. Snow (1961), Secondary particulate matter from meteor vapors, *J. Meteorol.*, *18*, 736–745.

Sassi, F., D. Kinnison, B. A. Boville, R. R. Garcia, and R. Roble (2004), Effect of El Niño-Southern Oscillation on the dynamical, thermal, and chemical structure of the middle atmosphere, *J. Geophys. Res.*, *109*, D17108, doi:10.1029/2003JD004434.

Schulte, P., and F. Arnold (1992), Detection of upper atmospheric negatively charged microclusters by a rocket borne mass spectrometer, *Geophys. Res. Lett.*, *19*, 2297–2300.

Singer, W., U. von Zahn, and J. Weiss (2004), Diurnal and annual variations of meteor rates at the artic circle, *Atmos. Chem. Phys.*, *4*, 1355–1363.

Siskind, D. E., and M. H. Stevens (2006), A radiative feedback from an interactive polar mesospheric cloud parameterization in a two dimensional model, *Adv. Space Res.*, *38*, 2383–2387.

Siskind, D. E., J. T. Bacmeister, M. E. Summers, and J. M. Russell III (1997), Two-dimensional model calculations of nitric oxide transport in the middle atmosphere and comparison with Halogen Occultation Experiment data, *J. Geophys. Res.*, *102*, 3527–3545.

Siskind, D. E., S. D. Eckermann, J. P. McCormack, M. J. Alexander, and J. T. Bacmeister (2003), Hemispheric differences in the temperature of the summertime stratosphere and mesosphere, *J. Geophys. Res.*, *108*(D2), 4051, doi:10.1029/2002JD002095.

Siskind, D. E., M. H. Stevens, and C. R. Englert (2005), A model study of global variability in mesospheric cloudiness, *J. Atmos. Sol. Terr. Phys.*, *67*, 501–513.

Siskind, D. E., M. Hervig, J. Gumbel, and M. H. Stevens (2007), Polar mesospheric cloud mass and the ice budget: 3. Application of a coupled ice-chemistry-dynamics model and comparison with observations, *J. Geophys. Res.*, *112*, D08303, doi:10.1029/2006JD007499.

Summers, M. E., and D. E. Siskind (1999), Surface recombination of O and H_2 on meteoric dust as a source of mesospheric water vapor, *Geophys. Res. Lett.*, *26*, 1837–1840.

Summers, M. E., D. E. Siskind, J. T. Bacmeister, R. R. Conway, S. E. Zasadil, and D. F. Strobel (1997), Seasonal variation of middle atmospheric CH_4 and H_2O with a new chemical dynamical model, *J. Geophys. Res.*, *102*, 3503–3526.

Szasz, C., J. Kero, and A. Pellinen-Wannberg (2005), Latitudional variations of diurnal meteor rates, *Earth Moon Planets*, *95*, 101–107.

Testa, J. P., J. R. Stephens, W. W. Berg, T. A. Cahill, T. Onaka, Y. Nakada, J. Arnold, N. Fong, and P. D. Sperry (1990), Collection of microparticles at high balloon altitides in the stratosphere, *Earth Planet. Sci. Lett.*, *98*, 287–302.

Toon, O. B., R. P. Turco, P. Hamill, C. S. Kiang, and R. C. Whitten (1979), A one dimensional model describing aerosol formation and evolution in the stratosphere, II. Sensitivity studies and comparison with observations., *J. Atmos. Sci.*, *36*, 718–736.

Toon, O. B., R. P. Turco, D. Westphal, R. Malone, and M. S. Liu (1988), A multidimensional model for aerosols: Description and computational analogs, *J. Atmos. Sci.*, *45*, 2123–2143.

Toon, O. B., R. P. Turco, J. Jordan, J. Goodman, and G. Ferry (1989), Physical processes in polar stratospheric clouds, *J. Geophys. Res.*, *94*, 11,359–11,380.

Turco, R. P., P. Hamill, O. B. Toon, R. C. Whitten, and C. S. Kiang (1979), A one dimensional model describing aerosol formation and evolution in the stratosphere, I. physical processes and mathematical analogs., *J. Atmos. Sci.*, *36*, 699–717.

Turco, R. P., O. B. Toon, R. C. Whitten, R. G. Keesee, and D. Hollenbach (1982), Noctilucent clouds: Simulation studies of their genesis, properties and global influences, *Planet. Space Sci.*, *3*, 1147–1181.

Vaida, V., H. G. Kjaergaard, P. Hintze, and D. J. Donaldson (2003), Photolysis of sulfuric acid vapor by visible solar radiation, *Science*, *299*, 1566–1568.

van de Hulst, H. C. (1957), *Light Scattering by Small Particles*, John Wiley, Hoboken, N. J.

Vaughan, G., and D. P. Wareing (2004), Stratospheric aerosol measurements by dual polarisation lidar, *Atmos. Chem. Phys.*, *4*, 6107–6126.

Voigt, C., et al. (2004), Nitric acid trihydrate (NAT) formation at low NAT supersaturation in polar stratospheric clouds (PSCs), *Atmos. Chem. Phys.*, *5*, 1371–1380.

von Zahn, U. (2005), The total mass flux of meteoroids into the Earth's upper atmosphere, *Eur. Space Agency Spec. Publ.*, *590*, 33–39.

Zhao, J., O. B. Toon, and R. P. Turco (1995), Origin of condensation nuclei in the springtime polar stratosphere, *J. Geophys. Res.*, *100*, 5215–5227.

J. Gumbel and L. Megner, Department of Meteorology, University of Stockholm, Svante Arrhenius väg 12, SE-10691 Stockholm, Sweden. (linda@misu.su.se)

M. Rapp, Leibniz-Institute of Atmospheric Physics, e.V. at University of Rostock, Schlossstrasse 6, D-18225 Khlungsborn, Germany.

D. E. Siskind, Space Science Division, Naval Research Laboratory, 4555 Overlook Avenue SW, Washington, DC 20375, USA.